

PriorDiffusion: Leverage Language Prior in Diffusion Models for Monocular Depth Estimation.

Ziyao Zeng¹ Jingcheng Ni² Daniel Wang¹ Patrick Rim¹
 Younjoon Chung¹ Fengyu Yang¹ Byung-Woo Hong³ Alex Wong¹

¹Yale University ²Duke Kunshan University ³Chung-Ang University³

¹{ziyao.zeng, daniel.wang.dhw33, patrick.rim, fengyu.yang}@yale.edu

¹{younjoon.chung, alex.wong}@yale.edu ²jn189@duke.edu ³hong@cau.ac.kr

Abstract

This paper explores the potential of leveraging language priors learned by text-to-image diffusion models to address ambiguity and visual nuisance in monocular depth estimation. Particularly, traditional monocular depth estimation suffers from inherent ambiguity due to the absence of stereo or multi-view depth cues, and nuisance due to lack of robustness of vision. We argue that language prior in diffusion models can enhance monocular depth estimation by leveraging the geometric prior aligned with the language description, which is learned during text-to-image pre-training. To generate images that reflect the text properly, the model must comprehend the size and shape of specified objects, their spatial relationship, and the scale of the scene. Thus, we propose PriorDiffusion, using a pre-trained text-to-image diffusion model that takes both image and text description that aligned with the scene to infer affine-invariant depth through a denoising process. We also show that language priors can guide the model’s attention to specific regions and help it perceive the 3D scene in alignment with user intent. Simultaneously, it acts as a constraint to accelerate the convergence of the diffusion trajectory, since learning 3D properties from a condensed, low-dimensional language feature is more efficient compared with learning from a redundant, high-dimensional image feature. By training on HyperSim and Virtual KITTI, we achieve state-of-the-art zero-shot performance and a faster convergence speed, compared with other diffusion-based depth estimators, across NYUv2, KITTI, ETH3D, and ScanNet.

1. Introduction

Monocular depth estimation requires the model to predict pixel-wise depth from a single image. Recent advancements in diffusion-based models have shown promise for generat-

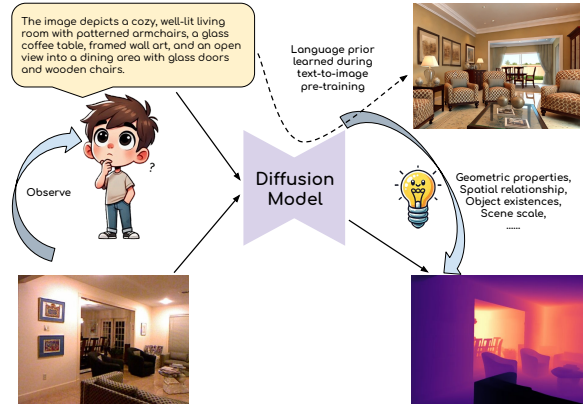


Figure 1. **Language prior in diffusion models enhances depth estimation** by leveraging the geometric prior aligned with the language description. It is learned during text-to-image generation pre-training, as to generate images under different viewpoints and layouts that accurately reflect the text, the model must comprehend the size and shape of specified objects, their spatial relationship, and the scale of the scene.

ing high-quality depth maps [12, 34, 35, 66, 67, 109] due to their ability to capture complex structures and fine details by progressively denoising a latent representation to produce accurate depth predictions. However, it remains a challenging task due to inherent ambiguities and various visual nuisances. One of the many inherent ambiguities is the scale ambiguity. Unlike stereo or multi-view depth estimation methods, monocular approaches lack the geometric depth cues provided by multiple perspectives, leading to difficulty in accurately discerning the relative sizes and distances of objects within a scene. That is, different real-world 3D scenes can project to the same 2D image under different scales. For example, a small object up close can appear identical to a larger object far away in an image. Another challenging ambiguity is texture ambiguity. Surfaces

that are uniformly textured or have repetitive patterns, like tiled floors, can create confusion for depth estimators. The models might misinterpret the repetition as uniform depth, even though the actual depth might vary (e.g., a tiled floor receding into the distance). Furthermore, visibility ambiguity creates limitations for discerning small, partial or occluded objects purely from the visual signal. On the other hand, visual nuisances such as illumination, motion blur, atmospheric conditions, and perspective distortion distort or obscure critical visual cues, leading vision algorithms to misinterpret scene structure, depth, and object boundaries, thus reducing their accuracy and reliability.

An emerging solution lies in leveraging language as a complementary modality to provide a prior to resolve ambiguity and visual nuisance. Language descriptions provided by humans offer a wealth of priors about spatial relationships, scene types, object sizes, and depth hierarchies. For example, distinguishing between a nearby toy car and a distant real car can be challenging for a model. However, when human-provided language inputs specify details like “This is a close toy car,” this serves as a prior that informs the model about the 3D size and shape of the object. Combined with the observed size, this prior helps narrow down the resolution space for depth estimation, leading to more accurate depth predictions. In cases where an object is small or partially occluded, language can indicate the object’s identity and semantics, enabling the model to infer its typical 3D size and shape and make more precise depth predictions for the observed portion. Language inputs are also valuable in resolving texture ambiguities. Descriptive cues can specify the type and function of surfaces in a scene, aiding the model in inferring geometric properties. For instance, if a uniformly textured surface is described as a “white ceiling,” the model can interpret it as a continuous, flat plane at a consistent depth above the observer, extending into the distance. Similarly, for surfaces with repetitive patterns, such as a red and black interwoven carpet, language inputs like “A red and black interwoven carpet extending across the room” can help the model recognize that the repeating pattern belongs to a flat surface, preventing misinterpretation of edges between tiles as depth discontinuities.

To this end, we propose PriorDiffusion, incorporating human-provided language descriptions of the scene as priors to guide the depth map predication. During text-to-image pre-training, diffusion models learn to generate diverse scenes that align with the provided language descriptions. To achieve this, the diffusion model must comprehend the size and shape of each object, their spatial relationship, and the scale of the scene described in the language input, to generate images that accurately represent the input text under various viewpoints and scene layouts. Thus, for depth estimation, the language priors provided by human-generated captions allow the model to leverage the

geometric priors embedded in the input text to more effectively perceive the 3D scene. In our PriorDiffusion, during the denoising process, both the image and the language input are used by the model to predict the noise to be removed. In the end, Gaussian noise is progressively refined into a depth map that aligns with both the input image and the language description. Given the difficulty of obtaining sufficient human-provided text descriptions for every training and inference image, we utilize a vision-language model, i.e. LLaVA [11], to generate descriptions for each image, simulating human annotation.

To support our hypothesis, we conduct training on two synthetic datasets, HyperSim [62] and Virtual KITTI [4], and conduct zero-shot evaluation on four real-world datasets, NYUv2 [69], KITTI [24], ETH3D [68], and ScanNet [10]. Comparing with other state-of-the-art diffusion depth estimators, we achieve superior qualitative results, and higher-fidelity quantitative results, with faster convergence speeds.

Our contributions. By leveraging language as a prior for monocular depth estimation using a diffusion model pre-trained with text-to-image generation, we demonstrate that:

- Language can provide a prior about the existence, geometric properties, and spatial relationships of objects specified in the language description, allowing depth estimators to better infer the depth of those objects.
- Language priors direct the model’s attention to specific regions, guiding it to perceive the 3D scene according to the user’s intent. This is particularly beneficial for regions that pose challenges to vision systems, such as those with small size, poor illumination, occlusion, or high visual similarity to the background.
- Language priors serve as a constraint to speed up the convergence of diffusion trajectory. Our intuition is that learning 3D properties like geometric characteristics and spatial relationships from a condensed, low-dimensional language feature is more efficient compared with learning from redundant, high-dimensional image features.

2. Related Work

Monocular depth estimation. Monocular depth estimation is a dense regression problem, requiring pixel-wise predictions of depth from a single image, capturing complex spatial relationships within the scene. Some depth models learn to infer pixel-wise depth in metric scale (i.e. meters) [2, 19, 36, 46, 80, 95, 96, 105] by minimizing loss between depth predictions and ground-truth depth maps. Each model typically applies to only one data domain in which it is trained, with similar camera parameters and object scales. Specifically, DORN [19] leverages a spacing-increasing discretization technique. AdaBins [2] partitions depth ranges into adaptive bins. NeWCRFs [95] uses neural window fully-connected CRFs to compute energy. VA-

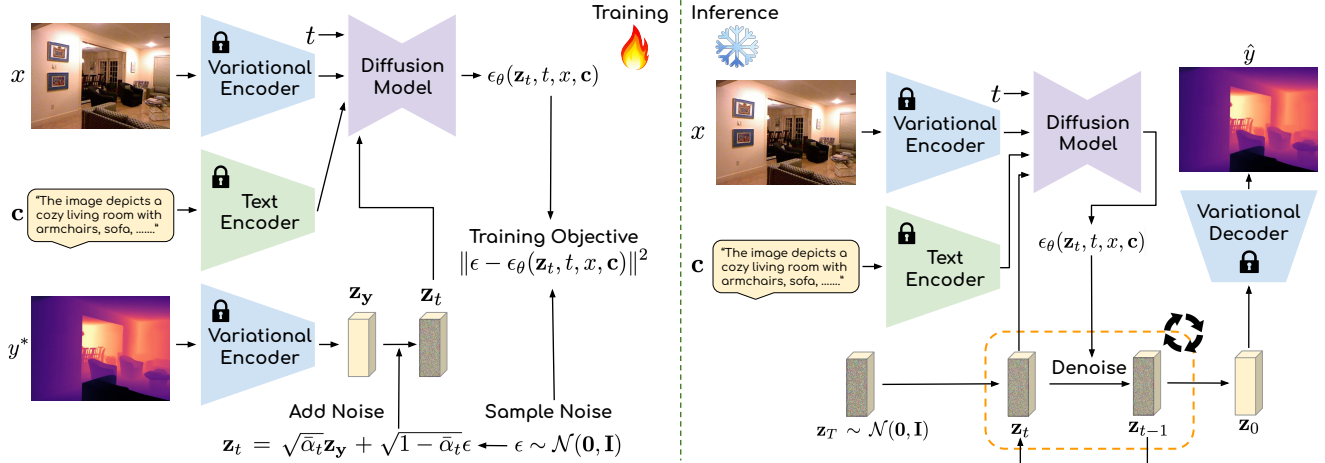


Figure 2. **Pipeline of PriorDiffusion.** We train the diffusion model to predict the noise added into the noisy depth latent \mathbf{z}_t at the time step t , based on \mathbf{z}_t , the input image x , and the corresponding language description c . During inference, the diffusion model predicts noise for \mathbf{z}_t at each time step and gradually denoise it from \mathbf{z}_T (pure Gaussian noise) into \mathbf{z}_0 (pure depth latent). Then \mathbf{z}_0 is decoded into the depth prediction using a frozen variational decoder.

DepthNet [46] uses first-order variational constraints, making the network aware of the depth gradient in the scene space. When ground-truth depth is not available, self-supervised approaches [3, 18, 33, 37, 38, 51, 55, 74, 76, 77, 79, 84, 94, 100, 106, 107, 111, 114] rely on geometric constraints, where scale is attributed through radar [70], inertials [28, 78], lidar [16, 49, 54, 81–83, 85, 91], or binocular images [23, 26, 27]. To enable generalization across diverse domains, empowering depth estimation in the wild, other works have explored affine-invariant depth estimation [13, 35, 45, 59, 60, 88, 89, 92, 93, 98], which predicts depth up to an unknown global shift and scale. This approach can accommodate varied scenes with different scales, while still preserving the geometric relationships between different objects or regions within the scene. HND [98] hierarchically normalizes the depth representations with spatial information and depth distributions. Depth Anything [88] learns from large-scale automatically annotated data. DPT [60] leverages vision transformers using a scale- and shift-invariant trimmed loss. MiDas [59] mixes multiple datasets with training objectives invariant to depth range and scale. Marigold [35] associates fine-tuning protocol with a diffusion model. Existing methods try to predict depth solely from images, which suffers from ambiguity like scale, object orientation, occlusion, and visual nuisance like viewpoints, illumination, appearance, texture, etc. On the other hand, our PriorDiffusion leverages language prior in Diffusion Models to provide a thorough understanding of the scene associated with the input text, to resolve the ambiguity and the nuisance variables in the visual algorithm.

Diffusion model for monocular depth estimation. Denoising Diffusion Probabilistic Model (DDPM) [30] learns

to reverse a diffusion process that progressively degrades images with Gaussian noise so that they can draw samples from the data distribution by applying the reverse process to random noise. They have been applied to various tasks like text-to-image generation [58, 63, 75, 117, 118], super resolution [22, 41, 64], image inpainting [9, 50, 90], 3D object generation [40, 48, 56], etc. Several approaches have explored the use of DDPM for metric depth estimation. DiffusionDepth [12] learns to denoise random depth distribution into a depth map with monocular visual conditions. Similarly, DDP [34] encodes the input image and use diffusion to decode it into a depth map. DepthGen [66] extends a multi-task diffusion model for metric depth prediction. Its successor, DDVM [67], focuses on pretraining with synthetic and real datasets to improve depth estimation performance. Lastly, VPD [109] and Marigold [35] utilizes a pretrained Stable Diffusion model [63] as an image feature extractor, incorporating additional text input for enhanced depth prediction. While previous works only focused on using images as conditions of diffusion models to predict depth, our PriorDiffusion utilizes language as priors in diffusion models to resolve ambiguity and visual nuisances, and conduct 3D perception in a controllable way.

Language for monocular depth estimation. Vision-Language models [5, 42, 43, 53, 57, 73] acquire a comprehensive understanding of languages and images through pre-training under diverse datasets, thereby establishing a robust foundation for downstream tasks. [7, 11, 17, 44, 72, 86, 87, 96, 97, 103–105, 116].

Typically, CLIP [57] employs contrastive learning on text-image pairs, enabling a range of applications like few-shot image classification [21, 101, 102, 113], image segmentation [61, 110], object detection [61, 115], and 3D

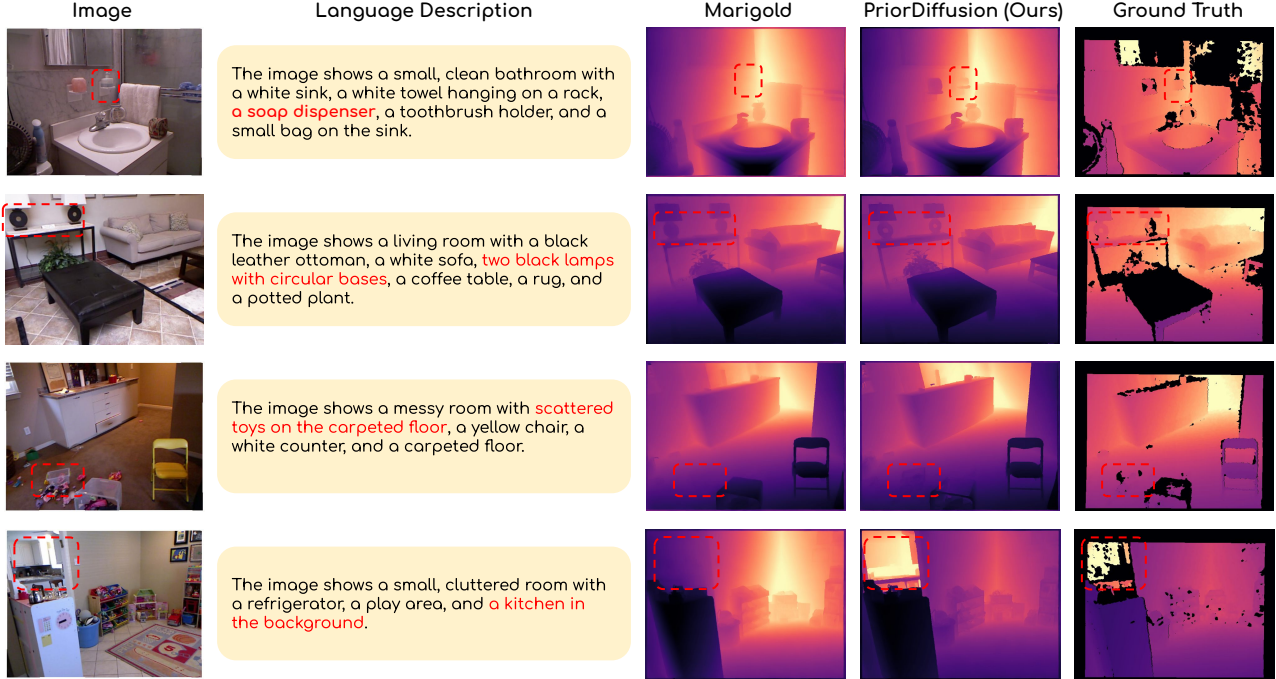


Figure 3. **Visualization on NYUv2.** Compared to Margold, our PriorDiffusion demonstrates more accurate depth prediction for a given input image, particularly for instances specified in the language description (marked in red). This is achieved by leveraging the language prior within the text-to-image diffusion model, enhancing the model’s ability to comprehend the geometric characteristics of these objects. Additionally, the language description directs the model’s attention to relevant regions, especially the ones that are easily neglected by visual signals, like “a soap dispenser” in the first row. It enables the depth estimator to perceive the 3D scene in a more controlled manner that aligns with the user’s interest.

perception [8, 29, 32, 99, 104, 105, 112, 116]. In light of their emerging ability, some works [1, 32, 105, 108] have tried to apply vision-language models for monocular depth estimation. Particularly, DepthCLIP [105] leverages the semantic depth response of CLIP with a depth projection scheme to conduct zero-shot monocular depth estimation. WorDepth [96] learned the variational prior distribution of 3D scenes from text captions. RSA [97] predict scale using language description to align relative depth to metric scale. While language has been applied in various aspects of 3D perception, our work is the first to use language priors in diffusion models to leverage the geometric prior aligned with the language description to enhance 3D perception.

3. Method

Problem setup. Given an RGB image $x : \Omega \subset \mathbb{R}^2 \rightarrow \mathbb{R}^3$, the goal of monocular depth estimation is to predict a dense depth map $y : \Omega \subset \mathbb{R}^2 \rightarrow \mathbb{R}_+$ using a parameterized function h , represented as a neural network, such that $y := h(\cdot)$. We utilize a supervised dataset $\mathcal{D} = \{x^{(m)}, \mathbf{c}^{(m)}, y^{*(m)}\}_{m=1}^M$ containing M samples, where $y^* : \Omega \subset \mathbb{R}^2 \rightarrow \mathbb{R}_+$ is the ground-truth depth map, and \mathbf{c} represents the text caption that describes the image.

Diffusion formulation. To use a diffusion model for monocular depth estimation, following [12, 34, 35, 66, 67, 109], we adopt the formulation of Denoising Diffusion Probabilistic Model (DDPM) [30]. We define a latent variable $\mathbf{z}_t \in \mathbb{R}^{H' \times W' \times C'}$ that represents a noisy version of the depth map in the latent space at diffusion timestep t . The ground-truth depth map y^* is encoded into a latent representation \mathbf{z}_y as supervision using a frozen VAE encoder E : $\mathbf{z}_y = E(y^*)$. The diffusion latent after the whole denoising process \mathbf{z}_0 is decoded back to the image space using the frozen VAE decoder D : $\hat{y} = D(\mathbf{z}_0)$.

Forward diffusion process. The forward process gradually adds noise to the latent depth feature in T steps. The process can be defined as:

$$q(\mathbf{z}_t | \mathbf{z}_{t-1}) = \mathcal{N}(\mathbf{z}_t; \sqrt{1 - \beta_t} \mathbf{z}_{t-1}, \beta_t \mathbf{I}),$$

where β_t is a scalar that defines the variance of the Gaussian noise added at each step t in the forward diffusion process. This parameter controls how much noise is added into the latent variable \mathbf{z}_t as it transitions from \mathbf{z}_{t-1} over time.

The forward process from y to \mathbf{z}_T can be written as:

$$q(\mathbf{z}_{1:T} | y^*) = \prod_{t=1}^T q(\mathbf{z}_t | \mathbf{z}_{t-1}),$$



Figure 4. **Visualization on KITTI.** Compared to Margold, our PriorDiffusion model shows superior accuracy in depth prediction for a given input image, especially for objects highlighted in the language description (marked in red), even when parts of the object are almost visible in the image (such as the parking car in the first column). This shows that the language prior can help the model better infer the geometric properties of these objects and improve distance estimation. Furthermore, the language descriptions guide the model’s attention to specific regions relevant to user needs, such as a sign at a distance, which can potentially enhance the safety of self-driving systems that rely solely on vision sensors.

where $D(\mathbf{z}_0) = \hat{y}$.

Reverse diffusion process. The goal of the reverse process is to denoise \mathbf{z}_T to recover \hat{y} . The reverse process is defined as:

$$p_{\theta}(\mathbf{z}_{0:T} | x, \mathbf{c}) = p(\mathbf{z}_T) \prod_{t=1}^T p_{\theta}(\mathbf{z}_{t-1} | \mathbf{z}_t, x, \mathbf{c}),$$

where $p(\mathbf{z}_T)$ is assumed to be a standard Gaussian distribution $\mathcal{N}(\mathbf{z}_T; \mathbf{0}, \mathbf{I})$, and the denoising step $p_{\theta}(\mathbf{z}_{t-1} | \mathbf{z}_t, x, \mathbf{c})$ is parameterized as:

$$p_{\theta}(\mathbf{z}_{t-1} | \mathbf{z}_t) = \mathcal{N}(\mathbf{z}_{t-1}; \mu_{\theta}(\mathbf{z}_t, t, x, \mathbf{c}), \Sigma_{\theta}(\mathbf{z}_t, t, x, \mathbf{c})),$$

where μ_{θ} and Σ_{θ} is the diffusion model, that predicts the mean and variance conditioned on \mathbf{z}_t , t , the input image x and the corresponding text \mathbf{c} . We use the U-Net from Stable Diffusion v2 [63] to initialize is the diffusion model. Specifically, given a text caption $\mathbf{c} = \{c_1, c_2, \dots\}$, we first encode it through a frozen CLIP text encoder, then feed it into the diffusion model. Given an image x , we encode it using the same VAE encoder $E(x)$ that encoded the depth map, concatenated with the depth latent \mathbf{z}_t , then feed it into the diffusion model.

Training objective. Our training objective is derived using the reparameterization trick and variational bounds, which involves predicting the noise added at each step. The loss

function is:

$$\mathcal{L}(\theta) = \mathbb{E}_{y, \epsilon, t} [\|\epsilon - \epsilon_{\theta}(\mathbf{z}_t, t, x, \mathbf{c})\|^2],$$

where: $\epsilon \sim \mathcal{N}(\mathbf{0}, \mathbf{I})$ is the noise sampled during the forward process, and $\mathbf{z}_t = \sqrt{\bar{\alpha}_t} \mathbf{z}_y + \sqrt{1 - \bar{\alpha}_t} \epsilon$ is the noisy depth map at step t , where $\bar{\alpha}_t = \prod_{s=1}^t (1 - \beta_s)$.

Inference. The inference phase begins by sampling a purely noisy latent variable \mathbf{z}_T from a standard Gaussian distribution, $\mathbf{z}_T \sim \mathcal{N}(\mathbf{0}, \mathbf{I})$. This initial noisy sample represents the starting point of the reverse diffusion process. The goal is to progressively refine this sample through a series of denoising steps until the final depth latent \mathbf{z}_0 is obtained. Each denoising step is to predict the noise component $\epsilon_{\theta}(\mathbf{z}_t, t, x, \mathbf{c})$ that needs to be removed from the latent variable at time step t . The prediction is made by the diffusion model conditioned on the noisy latent \mathbf{z}_t , the current timestep t , the input image x , and the corresponding text description \mathbf{c} . The iterative denoising process follows the reverse transition:

$$\mathbf{z}_{t-1} = \frac{1}{\sqrt{\alpha_t}} \left(\mathbf{z}_t - \frac{1 - \alpha_t}{\sqrt{1 - \bar{\alpha}_t}} \epsilon_{\theta}(\mathbf{z}_t, t, x, \mathbf{c}) \right),$$

where α_t and $\bar{\alpha}_t$ are derived from the noise schedule β_t . This reverse diffusion continues until $t = 0$, at which point the fully denoised latent \mathbf{z}_0 is reached. The predicted depth

Method	NYUv2		KITTI		ETH3D		ScanNet	
	$\delta_1 \uparrow$	AbsRel \downarrow	$\delta_1 \uparrow$	AbsRel \downarrow	$\delta_1 \uparrow$	AbsRel \downarrow	$\delta_1 \uparrow$	AbsRel \downarrow
DiverseDepth [92]	87.5	11.7	70.4	19.0	69.4	22.8	88.2	10.9
MiDaS [59]	88.5	11.1	63.0	23.6	75.2	18.4	84.6	12.1
LeReS [93]	91.6	9.0	78.4	14.9	77.7	17.1	91.7	9.1
Omnidata [13]	94.5	7.4	83.5	14.9	77.8	16.6	93.6	7.5
HDN [98]	94.8	6.9	86.7	11.5	83.3	12.1	93.9	8.0
DPT [60]	90.3	9.8	90.1	10.0	94.6	7.8	93.4	8.2
Marigold [35]	95.9	6.0	90.4	10.5	95.1	7.1	94.5	6.9
Marigold* (iter: 20000)	95.2	6.4	86.2	12.0	93.9	7.6	94.8	7.1
Marigold* (iter: 30000)	95.7	6.1	89.7	10.7	95.4	6.9	94.0	7.3
Ours (iter: 20000)	95.9	6.0	90.4	10.4	95.6	6.6	94.4	7.1
Ours (iter: 30000)	95.9	5.9	90.6	10.4	95.7	6.5	94.9	6.8

Table 1. **Quantitative Comparison.** We compare our PriorDiffusion against other state-of-the-art affine-invariant depth estimators across various zero-shot benchmarks. Metrics are reported as percentages. * indicates the results of the model that we re-implemented. Note that our method converges faster compared with Marigold, and is even better with only two-thirds iterations, attributing the language prior which provides a stronger constraint for the fast convergence of the diffusion trajectory.

map \hat{y} is obtained by decoding \mathbf{z}_0 back into the image space using the pre-trained and frozen VAE decoder: $\hat{y} = D(\mathbf{z}_0)$.

Obtain language description. To implement our method, we require human-provided text descriptions for each image. Since standard benchmarks do not include such descriptions, we propose using off-the-shelf models to generate text descriptions to simulate those a human would provide. To closely mimic human-like descriptions, we focus on natural text that is not constrained by templates and better resembles human input. For this purpose, we use the visual question-answering model LLaVA v1.6 Mistral [47]. We prompt this model with:

“Describe the image in one sentence, assuming it’s a real-world image. Pay close attention to objects, their spatial relationships, and the overall layout.”

This prompt is designed to elicit responses that include essential details, such as the positioning of objects, their interactions, and notable features that may impact depth estimation. Note that all training data we use are synthetic data, and by emphasizing “assuming it’s a real-world image,” we ensure that the descriptions align with the types of inputs and scenarios the model will encounter.

4. Experiments

Training datasets. We adopt the training scheme of Marigold [35], and train our PriorDiffusion on two synthetic datasets that cover both indoor and outdoor scenes. The first dataset, HyperSim [62], is a photorealistic collection of 461 indoor scenes. From this, we use the official split to select around 54K samples from 365 scenes, excluding any incomplete samples. RGB images and depth maps are resized to a resolution of 480×640 pixels, and the original distance measurements, relative to the focal point, are converted to conventional depth values relative to the focal plane. The

second dataset, Virtual KITTI [4, 20], includes synthetic street scenes from 5 settings with varied conditions, such as different weather and camera perspectives. We use the Virtual KITTI 2 [4] version. For training, we select four scenes, totaling approximately 20K samples, and crop the images to align with the KITTI benchmark resolution [24], setting the maximum depth to 80 meters.

Depth normalization for training. Following [35, 59, 60, 88], to standardize the ground truth depth maps \mathbf{d} , we apply a linear normalization ensuring that the depth values primarily fall within the range $[-1, 1]$, aligning with the input value range of the VAE. It ensures an affine-invariant depth representation that remains robust to data statistics, guaranteeing that all scenes are constrained by near and far planes with extreme depth values. The affine transformation for normalization is defined as:

$$\tilde{y}^* = \left(\frac{y^* - y_2}{y_2 - y_{98}} - 0.5 \right) \times 2, \quad (1)$$

where y_2 and y_{98} represent the 2% and 98% percentiles of the depth maps, respectively.

Evaluation datasets. We assess the performance of our PriorDiffusion using 4 real-world datasets that were not part of its training data, following the configuration as Marigold [35]. Both NYUv2 [69] and ScanNet [10] consist of indoor scenes captured with an RGB-D Kinect sensor. For NYUv2, we use the specified test set, containing 654 images. With ScanNet, we randomly select 800 images from the 312 official validation scenes for evaluation. The KITTI dataset [24, 25] features outdoor street scenes with sparse metric depth captured by a LiDAR sensor, where we apply the Eigen test split [14] consisting of 652 images, following the evaluation protocol of [15]. For ETH3D [68], which are also based on LiDAR measurements, we use all

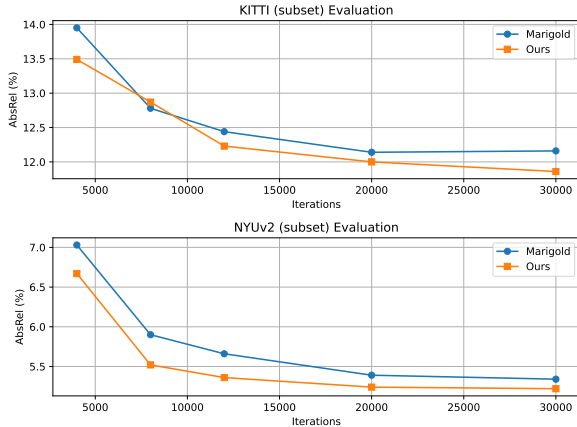


Figure 5. **Convergence speed comparison.** Our method converges faster during training compared with Marigold, since it’s more efficient to learn 3D property from condensed, low-dimensional language prior. Due to computation overhead, following the same configuration of Marigold, we use a subset of KITTI and NYUv2 for training-time evaluation.

454 samples that include ground truth depth maps.

Evaluation metric. Following the affine-invariant depth evaluation protocol [35, 59, 60, 88, 97], for each image and the predicted relative depth y , we fit a pair of scalars denoting the scale and shift parameters of the transformation: $(\hat{\alpha}, \hat{\beta}) = g_{\psi}(y, y^*) \in \mathbb{R}^2$. The metric depth prediction is obtained by $\hat{y} = \hat{\alpha} \cdot y + \hat{\beta}$ such that:

$$\psi^* = \arg \min_{\psi} \frac{1}{|M|} \sum_{(i,j) \in \Omega} M(i,j) |\hat{y}(i,j) - y(i,j)| \quad (2)$$

where $\hat{y} = \hat{\alpha} \cdot y + \hat{\beta}$ denotes the predicted metric-scale depth aligned from relative depth y , $(i, j) \in \Omega$ denotes an image coordinate, and $M : \Omega \mapsto \{0, 1\}$ denotes a binary mask indicating valid coordinates in the ground truth depth y^* with values greater than zero. Then, we follow [6, 46, 96, 97, 105] to evaluate using first-order threshold accuracy, calculated as:

$$\delta_1 = \% \text{ of } y(i, j) \text{ s.t. } \max\left(\frac{y(i, j)}{y^*(i, j)}, \frac{y^*(i, j)}{y(i, j)}\right) < 1.25 \quad (3)$$

and mean absolute relative error, calculated as:

$$AbsRel = \frac{1}{|M|} \sum_{(i,j) \in \Omega} \frac{|y^*(i, j) - y(i, j)|}{y^*(i, j)} \quad (4)$$

Implementation details. We implemented our method using PyTorch, employing Stable Diffusion v2 [63] as the backbone and adhering to the original pre-training setup with the v -objective [65]. During training, we used the DDPM noise scheduler [30] with 1000 diffusion steps,

Method	NYUv2		KITTI		ETH3D	
	$\delta_1 \uparrow$	AbsRel \downarrow	$\delta_1 \uparrow$	AbsRel \downarrow	$\delta_1 \uparrow$	AbsRel \downarrow
Blank text input	95.5	6.2	89.3	10.9	95.0	6.9
“An image”	95.7	6.1	89.8	10.7	95.1	6.8
Template A	95.8	6.0	89.9	10.7	95.3	6.8
Template B	95.7	6.1	89.8	10.7	95.2	6.8
Template C	95.8	6.1	89.8	10.7	95.3	6.8
Ours	95.9	5.9	90.6	10.4	95.7	6.5

Template A: ‘A complex 3D scene with varying objects at different distances.’
 Template B: ‘A structured environment with intricate patterns and designs that create depth and guide the eye through various focal points.’
 Template C: ‘An elaborate scene with overlapping objects that create a sense of distance and spatial hierarchy within the environment.’

Table 2. **Template prompt comparison.** Metrics are reported as percentages. PriorDiffusion can preserve performance when language input is not feasible thus using a fixed prompt instead.

while at inference time, the DDIM scheduler [71] was applied with 50 sampling steps. Our training process spanned 30000 iterations with a batch size of 32, achieved through gradient accumulation over 16 steps (batch size of 2 per step) to fit a single GPU. We optimized the model using the Adam optimizer with a learning rate of $3 \cdot 10^{-5}$ and included random horizontal flipping as data augmentation. Training to convergence (usually our method converges after 20000 iterations) required approximately 4 days on an Nvidia RTX 3090 GPU.

Quantitative comparison. In Table 1, we compare our PriorDiffusion against other state-of-the-art affine-invariant depth estimators across all those zero-shot benchmarks listed in the previous section. PriorDiffusion achieves the highest δ_1 accuracy and the lowest absolute relative error (AbsRel) on all tested datasets, including NYUv2, KITTI, ETH3D, and ScanNet. Notably, PriorDiffusion matches or surpasses top competitors such as Marigold and DPT, demonstrating strong generalization capabilities with an AbsRel of 5.9% and δ_1 of 95.9% on NYUv2, and comparable excellence across other benchmarks. This is attributed to the generalization ability of language due to its invariance and robustness across diverse 3D scenes. As shown in Figure 5, another significant advantage of PriorDiffusion is its faster convergence, compared to Marigold. In Table 1, even at 20,000 iterations, PriorDiffusion achieves performance metrics comparable to or better than Marigold’s results at 30,000 iterations. This can be attributed to the language prior integrated into our model, which provides additional semantic and geometric prior serving as extra constraint that speed up the convergence diffusion process. An intuitive explanation is that the model expends less effort in learning the geometric properties and spatial relationships of objects from the image, which is high-dimensional and computationally intensive to process. Instead, much of this feature is already embedded in the language input, where these features are represented in a condensed and low-dimensional format. Human-provided language serves

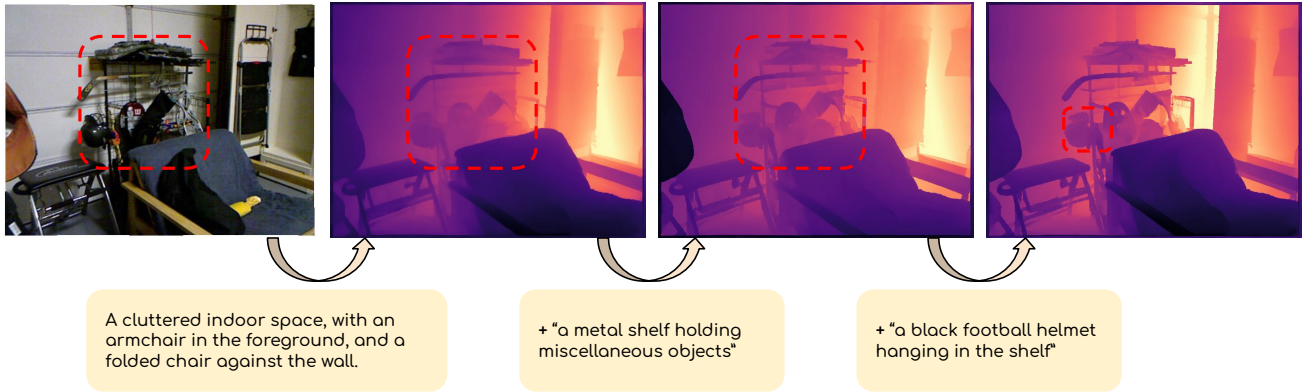


Figure 6. **Controllable depth estimation with language.** Each time, we append the newly added sentence to the end of the original sentence and repeat the inference process. It shows that by providing more details in the language, our method predicts more accurate depth for those specified regions or objects.

as an effective prior, allowing diffusion trajectory to converge more quickly.

Qualitative comparison. Besides the overall quantitative improvement, we claim that language prior can also guide the model’s attention to better perceive the region that is specified in the language description, which aligns more with users’ interests. The visualization for NYUv2 [69] is shown in Figure 3, where our PriorDiffusion achieves more accurate depth prediction for a given input image compared to Margold, especially for instances highlighted in the language description. For instance, in the first row, the soap dispenser is barely distinguishable in the input image due to its color and texture blending with the background. Vision-based depth estimators like Margold struggle to identify it, resulting in a depth prediction that matches the background. In contrast, the language description explicitly includes the term “a soap dispenser”, providing the model with a geometric and spatial prior that indicates the existence of a soap dispenser and what it should look like. Consequently, our PriorDiffusion can more accurately perceive the depth of the soap dispenser. Similarly, as shown in Figure 4, we visualize results for the KITTI [24] dataset, where objects such as a parked car or a sign are barely discernible from the visual signal alone. As shown in Figure 6, by incorporating more detailed language descriptions, depth predictions are enhanced for the specified regions or objects.

Template prompt comparison. In situations where user-provided descriptions are not available, we aim to explore whether our method can still perform effectively using either a blank input or standardized template prompts. If no specific language description that aligns with the scene is given by the user, we could instead use some pre-defined template prompt, such as “An image” or more elaborate prompts like, “A complex 3D scene with varying objects at different distances.”, as input of PriorDiffusion to main-

tain its performance.” These templates, as presented in Table 2, assist in preserving the model’s performance when language input is not practical. It is important to note that we did not account for meaningless language inputs during training and inference. Consequently, using template prompts as input during inference may differ from the training domain, leading to a significant covariate shift in language descriptions. This issue can be mitigated by incorporating template prompts as part of the input during training, enabling PriorDiffusion to better adapt to various scenarios where meaningful language descriptions are not feasible.

5. Discussion

Limitation. One primary limitation is its dependence on the accuracy and detail of the provided language descriptions. Ambiguous or misleading text inputs from human users can result in suboptimal depth predictions and potentially compromise the model’s performance. Additionally, the computational cost of training and inferring using diffusion models remains higher than that of other CNN or Transformer-based methods, which may affect the feasibility of deploying this approach in real-time or resource-constrained environments. Last, our method requires language input from users, which may not always be feasible. In cases where user-provided descriptions are unavailable, our method can still function with a standardized template prompt. Another potential solution is to generate language descriptions on the fly using a vision-language model [11], an image captioner [31], or by following methods like RSA [97] to create structured text from the output of vision models [39, 115]. While we have not explored this approach in this paper, it presents a promising avenue for future research.

Conclusion. We present PriorDiffusion, a novel approach that integrates language priors with diffusion models to

enhance monocular depth estimation. By leveraging geometric prior learned by text-to-image model that associated with language, PriorDiffusion overcomes traditional ambiguities and visual nuisances associated with monocular depth estimation, achieving state-of-the-art performance across various zero-shot benchmarks, while maintaining a faster convergence speed. We also highlights the potential of bridging the gap between visual perception and language understanding in vision-based AI systems.

References

- [1] Dylan Auty and Krystian Mikolajczyk. Learning to prompt clip for monocular depth estimation: Exploring the limits of human language. In Proceedings of the IEEE/CVF International Conference on Computer Vision, pages 2039–2047, 2023. 4
- [2] Shariq Farooq Bhat, Ibraheem Alhashim, and Peter Wonka. Adabins: Depth estimation using adaptive bins. In Proceedings of the IEEE/CVF Conference on Computer Vision and Pattern Recognition, pages 4009–4018, 2021. 2, 1
- [3] Jia-Wang Bian, Huangying Zhan, Naiyan Wang, Zhichao Li, Le Zhang, Chunhua Shen, Ming-Ming Cheng, and Ian Reid. Unsupervised scale-consistent depth learning from video. International Journal of Computer Vision, 129(9): 2548–2564, 2021. 3
- [4] Johann Cabon, Naila Murray, and Martin Humenberger. Virtual kitti 2. arXiv preprint arXiv:2001.10773, 2020. 2, 6, 1
- [5] Mathilde Caron, Hugo Touvron, Ishan Misra, Hervé Jégou, Julien Mairal, Piotr Bojanowski, and Armand Joulin. Emerging properties in self-supervised vision transformers. In Proceedings of the IEEE/CVF international conference on computer vision, pages 9650–9660, 2021. 3
- [6] Wenjie Chang, Yueyi Zhang, and Zhiwei Xiong. Transformer-based monocular depth estimation with attention supervision. In 32nd British Machine Vision Conference (BMVC 2021), 2021. 7
- [7] Jiaben Chen, Renrui Zhang, Dongze Lian, Jiaqi Yang, Ziyao Zeng, and Jianbo Shi. iquery: Instruments as queries for audio-visual sound separation. In Proceedings of the IEEE/CVF Conference on Computer Vision and Pattern Recognition, pages 14675–14686, 2023. 3
- [8] Runnan Chen, Youquan Liu, Lingdong Kong, Xinge Zhu, Yuexin Ma, Yikang Li, Yuenan Hou, Yu Qiao, and Wenping Wang. Clip2scene: Towards label-efficient 3d scene understanding by clip. In Proceedings of the IEEE/CVF Conference on Computer Vision and Pattern Recognition, pages 7020–7030, 2023. 4
- [9] Ciprian Corneanu, Raghudeep Gadde, and Aleix M Martinez. Latentpaint: Image inpainting in latent space with diffusion models. In Proceedings of the IEEE/CVF Winter Conference on Applications of Computer Vision, pages 4334–4343, 2024. 3
- [10] Angela Dai, Angel X Chang, Manolis Savva, Maciej Halber, Thomas Funkhouser, and Matthias Nießner. Scannet: Richly-annotated 3d reconstructions of indoor scenes. In Proceedings of the IEEE conference on computer vision and pattern recognition, pages 5828–5839, 2017. 2, 6, 1
- [11] Zhicheng Ding, Panfeng Li, Qikai Yang, and Siyang Li. Enhance image-to-image generation with llava-generated prompts. In 2024 5th International Conference on Information Science, Parallel and Distributed Systems (ISPDS), pages 77–81. IEEE, 2024. 2, 3, 8
- [12] Yiqun Duan, Xianda Guo, and Zheng Zhu. Diffusiondepth: Diffusion denoising approach for monocular depth estimation. arXiv preprint arXiv:2303.05021, 2023. 1, 3, 4
- [13] Ainaz Eftekhari, Alexander Sax, Jitendra Malik, and Amir Zamir. Omnidata: A scalable pipeline for making multi-task mid-level vision datasets from 3d scans. In Proceedings of the IEEE/CVF International Conference on Computer Vision, pages 10786–10796, 2021. 3, 6
- [14] David Eigen and Rob Fergus. Predicting depth, surface normals and semantic labels with a common multi-scale convolutional architecture. In Proceedings of the IEEE international conference on computer vision, pages 2650–2658, 2015. 6, 1
- [15] David Eigen, Christian Puhrsch, and Rob Fergus. Depth map prediction from a single image using a multi-scale deep network. Advances in neural information processing systems, 27, 2014. 6, 1
- [16] Vadim Ezhov, Hyoungseob Park, Zhaoyang Zhang, Rishi Upadhyay, Howard Zhang, Chethan Chinder Chandrappa, Achuta Kadambi, Yunhao Ba, Julie Dorsey, and Alex Wong. All-day depth completion. In 2023 IEEE/RSJ International Conference on Intelligent Robots and Systems (IROS). IEEE, 2024. 3
- [17] Xiaojing Fan and Chunliang Tao. Towards resilient and efficient llms: A comparative study of efficiency, performance, and adversarial robustness. arXiv preprint arXiv:2408.04585, 2024. 3
- [18] Xiaohan Fei, Alex Wong, and Stefano Soatto. Geosupervised visual depth prediction. IEEE Robotics and Automation Letters, 4(2):1661–1668, 2019. 3
- [19] Huan Fu, Mingming Gong, Chaohui Wang, Kayhan Batmanghelich, and Dacheng Tao. Deep ordinal regression network for monocular depth estimation. In Proceedings of the IEEE conference on computer vision and pattern recognition, pages 2002–2011, 2018. 2
- [20] Adrien Gaidon, Qiao Wang, Johann Cabon, and Eleonora Vig. Virtual worlds as proxy for multi-object tracking analysis. In Proceedings of the IEEE conference on Computer Vision and Pattern Recognition, pages 4340–4349, 2016. 6, 1
- [21] Peng Gao, Shijie Geng, Renrui Zhang, Teli Ma, Rongyao Fang, Yongfeng Zhang, Hongsheng Li, and Yu Qiao. Clip-adapter: Better vision-language models with feature adapters. arXiv preprint arXiv:2110.04544, 2021. 3
- [22] Sicheng Gao, Xuhui Liu, Bohan Zeng, Sheng Xu, Yanjing Li, Xiaoyan Luo, Jianzhuang Liu, Xiantong Zhen, and Baoshang Zhang. Implicit diffusion models for continuous super-resolution. In Proceedings of the IEEE/CVF conference on computer vision and pattern recognition, pages 10021–10030, 2023. 3

- [23] Ravi Garg, Vijay Kumar Bg, Gustavo Carneiro, and Ian Reid. Unsupervised cnn for single view depth estimation: Geometry to the rescue. In Computer Vision–ECCV 2016: 14th European Conference, Amsterdam, The Netherlands, October 11–14, 2016, Proceedings, Part VIII 14, pages 740–756. Springer, 2016. 3
- [24] Andreas Geiger, Philip Lenz, and Raquel Urtasun. Are we ready for autonomous driving? the kitti vision benchmark suite. In 2012 IEEE conference on computer vision and pattern recognition, pages 3354–3361. IEEE, 2012. 2, 6, 8, 1
- [25] Andreas Geiger, Philip Lenz, Christoph Stiller, and Raquel Urtasun. Vision meets robotics: The kitti dataset. The International Journal of Robotics Research, 32(11):1231–1237, 2013. 6, 1, 2
- [26] Clément Godard, Oisín Mac Aodha, and Gabriel J Brostow. Unsupervised monocular depth estimation with left-right consistency. In Proceedings of the IEEE conference on computer vision and pattern recognition, pages 270–279, 2017. 3
- [27] Clément Godard, Oisín Mac Aodha, Michael Firman, and Gabriel J Brostow. Digging into self-supervised monocular depth estimation. In Proceedings of the IEEE/CVF international conference on computer vision, pages 3828–3838, 2019. 3
- [28] Vitor Guizilini, Igor Vasiljevic, Rares Ambrus, Greg Shakhnarovich, and Adrien Gaidon. Full surround monodepth from multiple cameras. IEEE Robotics and Automation Letters, 7(2):5397–5404, 2022. 3
- [29] Deepti Hegde, Jeya Maria Jose Valanarasu, and Vishal Patel. Clip goes 3d: Leveraging prompt tuning for language grounded 3d recognition. In Proceedings of the IEEE/CVF International Conference on Computer Vision, pages 2028–2038, 2023. 4
- [30] Jonathan Ho, Ajay Jain, and Pieter Abbeel. Denoising diffusion probabilistic models. Advances in neural information processing systems, 33:6840–6851, 2020. 3, 4, 7, 2
- [31] Jia Cheng Hu, Roberto Cavicchioli, and Alessandro Capotondi. Expansionnet v2: Block static expansion in fast end to end training for image captioning. arXiv preprint arXiv:2208.06551, 2022. 8
- [32] Xueting Hu, Ce Zhang, Yi Zhang, Bowen Hai, Ke Yu, and Zhihai He. Learning to adapt clip for few-shot monocular depth estimation. arXiv preprint arXiv:2311.01034, 2023. 4
- [33] Pan Ji, Runze Li, Bir Bhanu, and Yi Xu. Monoindoor: Towards good practice of self-supervised monocular depth estimation for indoor environments. In Proceedings of the IEEE/CVF International Conference on Computer Vision, pages 12787–12796, 2021. 3
- [34] Yuanfeng Ji, Zhe Chen, Enze Xie, Lanqing Hong, Xihui Liu, Zhaoqiang Liu, Tong Lu, Zhenguo Li, and Ping Luo. Ddp: Diffusion model for dense visual prediction. In Proceedings of the IEEE/CVF International Conference on Computer Vision, pages 21741–21752, 2023. 1, 3, 4
- [35] Bingxin Ke, Anton Obukhov, Shengyu Huang, Nando Metzger, Rodrigo Caye Daudt, and Konrad Schindler. Repurposing diffusion-based image generators for monocular depth estimation. arXiv preprint arXiv:2312.02145, 2023. 1, 3, 4, 6, 7, 2
- [36] Dong Lao, Yangchao Wu, Tian Yu Liu, Alex Wong, and Stefano Soatto. Sub-token vit embedding via stochastic resonance transformers. In International Conference on Machine Learning. PMLR, 2024. 2
- [37] Dong Lao, Fengyu Yang, Daniel Wang, Hyungseob Park, Samuel Lu, Alex Wong, and Stefano Soatto. On the viability of monocular depth pre-training for semantic segmentation. In European Conference on Computer Vision. Springer, 2024. 3
- [38] Boying Li, Yuan Huang, Zeyu Liu, Danping Zou, and Wenxian Yu. Structdepth: Leveraging the structural regularities for self-supervised indoor depth estimation. In Proceedings of the IEEE/CVF International Conference on Computer Vision, pages 12663–12673, 2021. 3
- [39] Feng Li, Hao Zhang, Huaizhe Xu, Shilong Liu, Lei Zhang, Lionel M Ni, and Heung-Yeung Shum. Mask dino: Towards a unified transformer-based framework for object detection and segmentation. In Proceedings of the IEEE/CVF Conference on Computer Vision and Pattern Recognition, pages 3041–3050, 2023. 8
- [40] Gang Li, Heliang Zheng, Chaoyue Wang, Chang Li, Changwen Zheng, and Dacheng Tao. 3ddesigner: Towards photorealistic 3d object generation and editing with text-guided diffusion models. arXiv preprint arXiv:2211.14108, 2022. 3
- [41] Haoying Li, Yifan Yang, Meng Chang, Shiqi Chen, Huajun Feng, Zhihai Xu, Qi Li, and Yueting Chen. Srdiff: Single image super-resolution with diffusion probabilistic models. Neurocomputing, 479:47–59, 2022. 3
- [42] Junnan Li, Dongxu Li, Caiming Xiong, and Steven Hoi. Blip: Bootstrapping language-image pre-training for unified vision-language understanding and generation. In International Conference on Machine Learning, pages 12888–12900. PMLR, 2022. 3
- [43] Junnan Li, Dongxu Li, Silvio Savarese, and Steven Hoi. Blip-2: Bootstrapping language-image pre-training with frozen image encoders and large language models. arXiv preprint arXiv:2301.12597, 2023. 3
- [44] Panfeng Li, Qikai Yang, Xieming Geng, Wenjing Zhou, Zhicheng Ding, and Yi Nian. Exploring diverse methods in visual question answering. In 2024 5th International Conference on Electronic Communication and Artificial Intelligence (ICECAD), pages 681–685. IEEE, 2024. 3
- [45] Zhengqi Li and Noah Snavely. Megadepth: Learning single-view depth prediction from internet photos. In Proceedings of the IEEE conference on computer vision and pattern recognition, pages 2041–2050, 2018. 3
- [46] Ce Liu, Suryansh Kumar, Shuhang Gu, Radu Timofte, and Luc Van Gool. Va-depthnet: A variational approach to single image depth prediction. arXiv preprint arXiv:2302.06556, 2023. 2, 3, 7
- [47] Haotian Liu, Chunyuan Li, Yuheng Li, and Yong Jae Lee. Improved baselines with visual instruction tuning, 2023. 6, 2

- [48] Minghua Liu, Ruoxi Shi, Linghao Chen, Zhuoyang Zhang, Chao Xu, Xinyue Wei, Hansheng Chen, Chong Zeng, Jiayuan Gu, and Hao Su. One-2-3-45++: Fast single image to 3d objects with consistent multi-view generation and 3d diffusion. In Proceedings of the IEEE/CVF Conference on Computer Vision and Pattern Recognition, pages 10072–10083, 2024. 3
- [49] Tian Yu Liu, Parth Agrawal, Allison Chen, Byung-Woo Hong, and Alex Wong. Monitored distillation for positive congruent depth completion. In Computer Vision–ECCV 2022: 17th European Conference, Tel Aviv, Israel, October 23–27, 2022, Proceedings, Part II, pages 35–53. Springer, 2022. 3
- [50] Andreas Lugmayr, Martin Danelljan, Andres Romero, Fisher Yu, Radu Timofte, and Luc Van Gool. Repaint: Inpainting using denoising diffusion probabilistic models. In Proceedings of the IEEE/CVF conference on computer vision and pattern recognition, pages 11461–11471, 2022. 3
- [51] Reza Mahjourian, Martin Wicke, and Anelia Angelova. Un-supervised learning of depth and ego-motion from monocular video using 3d geometric constraints. In Proceedings of the IEEE conference on computer vision and pattern recognition, pages 5667–5675, 2018. 3
- [52] OpenAI. Chatgpt-4: Conversational ai model, 2024. Accessed via OpenAI’s platform for generating and refining content. 2
- [53] Maxime Oquab, Timothée Darcet, Théo Moutakanni, Huy Vo, Marc Szafraniec, Vasil Khalidov, Pierre Fernandez, Daniel Haziza, Francisco Massa, Alaaeldin El-Nouby, et al. Dinov2: Learning robust visual features without supervision. arXiv preprint arXiv:2304.07193, 2023. 3
- [54] Hyungseob Park, Anjali Gupta, and Alex Wong. Test-time adaptation for depth completion. In Proceedings of the IEEE/CVF Conference on Computer Vision and Pattern Recognition, pages 20519–20529, 2024. 3
- [55] Rui Peng, Ronggang Wang, Yawen Lai, Luyang Tang, and Yangang Cai. Excavating the potential capacity of self-supervised monocular depth estimation. In Proceedings of the IEEE/CVF International Conference on Computer Vision, pages 15560–15569, 2021. 3
- [56] Guocheng Qian, Jinjie Mai, Abdullah Hamdi, Jian Ren, Aliaksandr Siarohin, Bing Li, Hsin-Ying Lee, Ivan Skokhodov, Peter Wonka, Sergey Tulyakov, et al. Magic123: One image to high-quality 3d object generation using both 2d and 3d diffusion priors. arXiv preprint arXiv:2306.17843, 2023. 3
- [57] Alec Radford, Jong Wook Kim, Chris Hallacy, Aditya Ramesh, Gabriel Goh, Sandhini Agarwal, Girish Sastry, Amanda Askell, Pamela Mishkin, Jack Clark, et al. Learning transferable visual models from natural language supervision. In International conference on machine learning, pages 8748–8763. PMLR, 2021. 3
- [58] Aditya Ramesh, Prafulla Dhariwal, Alex Nichol, Casey Chu, and Mark Chen. Hierarchical text-conditional image generation with clip latents. arXiv preprint arXiv:2204.06125, 1(2):3, 2022. 3
- [59] René Ranftl, Katrin Lasinger, David Hafner, Konrad Schindler, and Vladlen Koltun. Towards robust monocular depth estimation: Mixing datasets for zero-shot cross-dataset transfer. IEEE transactions on pattern analysis and machine intelligence, 44(3):1623–1637, 2020. 3, 6, 7
- [60] René Ranftl, Alexey Bochkovskiy, and Vladlen Koltun. Vision transformers for dense prediction. In Proceedings of the IEEE/CVF international conference on computer vision, pages 12179–12188, 2021. 3, 6, 7
- [61] Yongming Rao, Wenliang Zhao, Guangyi Chen, Yansong Tang, Zheng Zhu, Guan Huang, Jie Zhou, and Jiwen Lu. Denseclip: Language-guided dense prediction with context-aware prompting. arXiv preprint arXiv:2112.01518, 2021. 3
- [62] Mike Roberts, Jason Ramapuram, Anurag Ranjan, Atulit Kumar, Miguel Angel Bautista, Nathan Paczan, Russ Webb, and Joshua M Susskind. Hypersim: A photorealistic synthetic dataset for holistic indoor scene understanding. In Proceedings of the IEEE/CVF international conference on computer vision, pages 10912–10922, 2021. 2, 6, 1
- [63] Robin Rombach, Andreas Blattmann, Dominik Lorenz, Patrick Esser, and Björn Ommer. High-resolution image synthesis with latent diffusion models. In Proceedings of the IEEE/CVF conference on computer vision and pattern recognition, pages 10684–10695, 2022. 3, 5, 7, 2
- [64] Chitwan Saharia, Jonathan Ho, William Chan, Tim Salimans, David J Fleet, and Mohammad Norouzi. Image super-resolution via iterative refinement. IEEE transactions on pattern analysis and machine intelligence, 45(4):4713–4726, 2022. 3
- [65] Tim Salimans and Jonathan Ho. Progressive distillation for fast sampling of diffusion models. arXiv preprint arXiv:2202.00512, 2022. 7, 2
- [66] Saurabh Saxena, Abhishek Kar, Mohammad Norouzi, and David J Fleet. Monocular depth estimation using diffusion models. arXiv preprint arXiv:2302.14816, 2023. 1, 3, 4
- [67] Saurabh Saxena, Charles Herrmann, Junhwa Hur, Abhishek Kar, Mohammad Norouzi, Deqing Sun, and David J Fleet. The surprising effectiveness of diffusion models for optical flow and monocular depth estimation. Advances in Neural Information Processing Systems, 36, 2024. 1, 3, 4
- [68] Thomas Schops, Johannes L Schonberger, Silvano Galliani, Torsten Sattler, Konrad Schindler, Marc Pollefeys, and Andreas Geiger. A multi-view stereo benchmark with high-resolution images and multi-camera videos. In Proceedings of the IEEE conference on computer vision and pattern recognition, pages 3260–3269, 2017. 2, 6, 1
- [69] Nathan Silberman, Derek Hoiem, Pushmeet Kohli, and Rob Fergus. Indoor segmentation and support inference from rgbd images. In Computer Vision–ECCV 2012: 12th European Conference on Computer Vision, Florence, Italy, October 7-13, 2012, Proceedings, Part V 12, pages 746–760. Springer, 2012. 2, 6, 8, 1
- [70] Akash Deep Singh, Yunhao Ba, Ankur Sarker, Howard Zhang, Achuta Kadambi, Stefano Soatto, Mani Srivastava, and Alex Wong. Depth estimation from camera image and mmwave radar point cloud. In Proceedings of the

- IEEE/CVF Conference on Computer Vision and Pattern Recognition, pages 9275–9285, 2023. 3
- [71] Jiaming Song, Chenlin Meng, and Stefano Ermon. Denoising diffusion implicit models. arXiv preprint arXiv:2010.02502, 2020. 7, 2
- [72] Chunliang Tao, Xiaojing Fan, and Yahe Yang. Harnessing llms for api interactions: A framework for classification and synthetic data generation. arXiv preprint arXiv:2409.11703, 2024. 3
- [73] Yiyi Tao, Zhuoyue Wang, Hang Zhang, and Lun Wang. Nevlp: Noise-robust framework for efficient vision-language pre-training. arXiv preprint arXiv:2409.09582, 2024. 3
- [74] Rishi Upadhyay, Howard Zhang, Yunhao Ba, Ethan Yang, Blake Gella, Sicheng Jiang, Alex Wong, and Achuta Kadambi. Enhancing diffusion models with 3d perspective geometry constraints. ACM Transactions on Graphics (TOG), 42(6):1–15, 2023. 3
- [75] Ruoyu Wang, Yongqi Yang, Zhihao Qian, Ye Zhu, and Yu Wu. Diffusion in diffusion: Cyclic one-way diffusion for text-vision-conditioned generation. arXiv preprint arXiv:2306.08247, 2023. 3
- [76] Ruoyu Wang, Zehao Yu, and Shenghua Gao. Planedepth: Self-supervised depth estimation via orthogonal planes. In Proceedings of the IEEE/CVF Conference on Computer Vision and Pattern Recognition, pages 21425–21434, 2023. 3
- [77] Youhong Wang, Yunji Liang, Hao Xu, Shaohui Jiao, and Hongkai Yu. Sqldepth: Generalizable self-supervised fine-structured monocular depth estimation. arXiv preprint arXiv:2309.00526, 2023. 3
- [78] Yi Wei, Linqing Zhao, Wenzhao Zheng, Zheng Zhu, Yongming Rao, Guan Huang, Jiwen Lu, and Jie Zhou. Surrounddepth: Entangling surrounding views for self-supervised multi-camera depth estimation. In Conference on Robot Learning, pages 539–549. PMLR, 2023. 3
- [79] Alex Wong and Stefano Soatto. Bilateral cyclic constraint and adaptive regularization for unsupervised monocular depth prediction. In Proceedings of the IEEE/CVF Conference on Computer Vision and Pattern Recognition, pages 5644–5653, 2019. 3
- [80] Alex Wong, Safa Cicek, and Stefano Soatto. Targeted adversarial perturbations for monocular depth prediction. Advances in neural information processing systems, 33: 8486–8497, 2020. 2
- [81] Alex Wong, Xiaohan Fei, Stephanie Tsuei, and Stefano Soatto. Unsupervised depth completion from visual inertial odometry. IEEE Robotics and Automation Letters, 5(2):1899–1906, 2020. 3
- [82] Alex Wong, Safa Cicek, and Stefano Soatto. Learning topology from synthetic data for unsupervised depth completion. IEEE Robotics and Automation Letters, 6(2): 1495–1502, 2021.
- [83] Alex Wong, Xiaohan Fei, Byung-Woo Hong, and Stefano Soatto. An adaptive framework for learning unsupervised depth completion. IEEE Robotics and Automation Letters, 6(2):3120–3127, 2021. 3
- [84] Cho-Ying Wu, Jialiang Wang, Michael Hall, Ulrich Neumann, and Shuochen Su. Toward practical monocular indoor depth estimation. In Proceedings of the IEEE/CVF Conference on Computer Vision and Pattern Recognition, pages 3814–3824, 2022. 3
- [85] Yangchao Wu, Tian Yu Liu, Hyouneseob Park, Stefano Soatto, Dong Lao, and Alex Wong. Augundo: Scaling up augmentations for monocular depth completion and estimation. In European Conference on Computer Vision. Springer, 2024. 3
- [86] Fengyu Yang, Chao Feng, Ziyang Chen, Hyouneseob Park, Daniel Wang, Yiming Dou, Ziyao Zeng, Xien Chen, Rit Gangopadhyay, Andrew Owens, and Alex Wong. Binding touch to everything: Learning unified multimodal tactile representations. In Proceedings of the IEEE/CVF Conference on Computer Vision and Pattern Recognition, 2024. 3
- [87] Fengyu Yang, Chao Feng, Daniel Wang, Tianye Wang, Ziyao Zeng, Zhiyang Xu, Hyouneseob Park, Pengliang Ji, Hanbin Zhao, Yuanning Li, et al. Neurobind: Towards unified multimodal representations for neural signals. arXiv preprint arXiv:2407.14020, 2024. 3
- [88] Lihe Yang, Bingyi Kang, Zilong Huang, Xiaogang Xu, Jiashi Feng, and Hengshuang Zhao. Depth anything: Unleashing the power of large-scale unlabeled data. arXiv preprint arXiv:2401.10891, 2024. 3, 6, 7
- [89] Lihe Yang, Bingyi Kang, Zilong Huang, Zhen Zhao, Xiaogang Xu, Jiashi Feng, and Hengshuang Zhao. Depth anything v2. arXiv preprint arXiv:2406.09414, 2024. 3
- [90] Shiyuan Yang, Xiaodong Chen, and Jing Liao. Uni-paint: A unified framework for multimodal image inpainting with pretrained diffusion model. In Proceedings of the 31st ACM International Conference on Multimedia, pages 3190–3199, 2023. 3
- [91] Yanchao Yang, Alex Wong, and Stefano Soatto. Dense depth posterior (ddp) from single image and sparse range. In Proceedings of the IEEE/CVF Conference on Computer Vision and Pattern Recognition, pages 3353–3362, 2019. 3
- [92] Wei Yin, Xinlong Wang, Chunhua Shen, Yifan Liu, Zhi Tian, Songcen Xu, Changming Sun, and Dou Renyin. Diversedepth: Affine-invariant depth prediction using diverse data. arXiv preprint arXiv:2002.00569, 2020. 3, 6
- [93] Wei Yin, Jianming Zhang, Oliver Wang, Simon Niklaus, Long Mai, Simon Chen, and Chunhua Shen. Learning to recover 3d scene shape from a single image. In Proceedings of the IEEE/CVF Conference on Computer Vision and Pattern Recognition, pages 204–213, 2021. 3, 6
- [94] Zehao Yu, Lei Jin, and Shenghua Gao. P 2 net: Patch-match and plane-regularization for unsupervised indoor depth estimation. In European Conference on Computer Vision, pages 206–222. Springer, 2020. 3
- [95] Weihao Yuan, Xiaodong Gu, Zuozhuo Dai, Siyu Zhu, and Ping Tan. Neural window fully-connected crfs for monocular depth estimation. In Proceedings of the IEEE/CVF Conference on Computer Vision and Pattern Recognition, pages 3916–3925, 2022. 2, 1
- [96] Ziyao Zeng, Daniel Wang, Fengyu Yang, Hyouneseob Park, Stefano Soatto, Dong Lao, and Alex Wong.

- Wordepth: Variational language prior for monocular depth estimation. In Proceedings of the IEEE/CVF Conference on Computer Vision and Pattern Recognition, pages 9708–9719, 2024. 2, 3, 4, 7
- [97] Ziyao Zeng, Yangchao Wu, Hyungseob Park, Daniel Wang, Fengyu Yang, Stefano Soatto, Dong Lao, Byung-Woo Hong, and Alex Wong. Rsa: Resolving scale ambiguities in monocular depth estimators through language descriptions. arXiv preprint arXiv:2410.02924, 2024. 3, 4, 7, 8, 1
- [98] Chi Zhang, Wei Yin, Billzb Wang, Gang Yu, Bin Fu, and Chunhua Shen. Hierarchical normalization for robust monocular depth estimation. Advances in Neural Information Processing Systems, 35:14128–14139, 2022. 3, 6
- [99] Junbo Zhang, Runpei Dong, and Kaisheng Ma. Clip-fo3d: Learning free open-world 3d scene representations from 2d dense clip. In Proceedings of the IEEE/CVF International Conference on Computer Vision, pages 2048–2059, 2023. 4
- [100] Mingliang Zhang, Xinchun Ye, Xin Fan, and Wei Zhong. Unsupervised depth estimation from monocular videos with hybrid geometric-refined loss and contextual attention. Neurocomputing, 379:250–261, 2020. 3
- [101] Renrui Zhang, Rongyao Fang, Peng Gao, Wei Zhang, Kunchang Li, Jifeng Dai, Yu Qiao, and Hongsheng Li. Tip-adapter: Training-free clip-adapter for better vision-language modeling. arXiv preprint arXiv:2111.03930, 2021. 3
- [102] Renrui Zhang, Longtian Qiu, Wei Zhang, and Ziyao Zeng. Vt-clip: Enhancing vision-language models with visual-guided texts. arXiv preprint arXiv:2112.02399, 2021. 3
- [103] Renrui Zhang, Ziyao Zeng, Ziyu Guo, Xinben Gao, Kexue Fu, and Jianbo Shi. Dspoint: Dual-scale point cloud recognition with high-frequency fusion. arXiv preprint arXiv:2111.10332, 2021. 3
- [104] Renrui Zhang, Ziyu Guo, Wei Zhang, Kunchang Li, Xupeng Miao, Bin Cui, Yu Qiao, Peng Gao, and Hongsheng Li. Pointclip: Point cloud understanding by clip. In Proceedings of the IEEE/CVF Conference on Computer Vision and Pattern Recognition, pages 8552–8562, 2022. 4
- [105] Renrui Zhang, Ziyao Zeng, Ziyu Guo, and Yafeng Li. Can language understand depth? In Proceedings of the 30th ACM International Conference on Multimedia, pages 6868–6874, 2022. 2, 3, 4, 7
- [106] Chaoqiang Zhao, Youmin Zhang, Matteo Poggi, Fabio Tosi, Xianda Guo, Zheng Zhu, Guan Huang, Yang Tang, and Stefano Mattoccia. Monovit: Self-supervised monocular depth estimation with a vision transformer. In 2022 International Conference on 3D Vision (3DV), pages 668–678. IEEE, 2022. 3
- [107] Wang Zhao, Shaohui Liu, Yezhi Shu, and Yong-Jin Liu. Towards better generalization: Joint depth-pose learning without posenet. In Proceedings of the IEEE/CVF Conference on Computer Vision and Pattern Recognition, pages 9151–9161, 2020. 3
- [108] Wenliang Zhao, Yongming Rao, Zuyan Liu, Benlin Liu, Jie Zhou, and Jiwen Lu. Unleashing text-to-image diffusion models for visual perception. arXiv preprint arXiv:2303.02153, 2023. 4
- [109] Wenliang Zhao, Yongming Rao, Zuyan Liu, Benlin Liu, Jie Zhou, and Jiwen Lu. Unleashing text-to-image diffusion models for visual perception. In Proceedings of the IEEE/CVF International Conference on Computer Vision, pages 5729–5739, 2023. 1, 3, 4
- [110] Chong Zhou, Chen Change Loy, and Bo Dai. Dense-clip: Extract free dense labels from clip. arXiv preprint arXiv:2112.01071, 2021. 3
- [111] Junsheng Zhou, Yuwang Wang, Kaihuai Qin, and Wenjun Zeng. Moving indoor: Unsupervised video depth learning in challenging environments. In Proceedings of the IEEE/CVF International Conference on Computer Vision, pages 8618–8627, 2019. 3
- [112] Junsheng Zhou, Jinsheng Wang, Baorui Ma, Yu-Shen Liu, Tiejun Huang, and Xinlong Wang. Uni3d: Exploring unified 3d representation at scale. arXiv preprint arXiv:2310.06773, 2023. 4
- [113] Kaiyang Zhou, Jingkang Yang, Chen Change Loy, and Ziwei Liu. Learning to prompt for vision-language models. arXiv preprint arXiv:2109.01134, 2021. 3
- [114] Tinghui Zhou, Matthew Brown, Noah Snavely, and David G Lowe. Unsupervised learning of depth and egomotion from video. In Proceedings of the IEEE conference on computer vision and pattern recognition, pages 1851–1858, 2017. 3
- [115] Xingyi Zhou, Rohit Girdhar, Armand Joulin, Philipp Krähenbühl, and Ishan Misra. Detecting twenty-thousand classes using image-level supervision. In European Conference on Computer Vision, pages 350–368. Springer, 2022. 3, 8
- [116] Xiangyang Zhu, Renrui Zhang, Bowei He, Ziyu Guo, Ziyao Zeng, Zipeng Qin, Shanghang Zhang, and Peng Gao. Pointclip v2: Prompting clip and gpt for powerful 3d open-world learning. In Proceedings of the IEEE/CVF International Conference on Computer Vision, pages 2639–2650, 2023. 3, 4
- [117] Ye Zhu, Yu Wu, Kyle Olszewski, Jian Ren, Sergey Tulyakov, and Yan Yan. Discrete contrastive diffusion for cross-modal music and image generation. arXiv preprint arXiv:2206.07771, 2022. 3
- [118] Ye Zhu, Yu Wu, Zhiwei Deng, Olga Russakovsky, and Yan Yan. Boundary guided learning-free semantic control with diffusion models. Advances in Neural Information Processing Systems, 36, 2024. 3

PriorDiffusion: Leverage Language Prior in Diffusion Models for Monocular Depth Estimation.

Supplementary Material

A. Dataset Details

We train our model on two synthetic datasets, Hypersim [62] and Virtual Kitti [4], and conduct zero-shot evaluations on four additional real-world datasets that were not part of its training data, NYUv2 [69], KITTI [24], ScanNet [10], and ETH3D [68]. Details of each dataset are provided below.

A.1. Training Datasets

Hypersim [62] is a photorealistic synthetic dataset designed for comprehensive indoor scene understanding, and is introduced since obtaining per-pixel ground truth labels from real images is often challenging or impossible for many essential scene understanding tasks. This dataset is created using a vast collection of synthetic scenes developed by professional artists, resulting in 77,400 images across 461 indoor scenes with detailed per-pixel annotations and corresponding ground truth geometry. HyperSim is built exclusively using publicly accessible 3D assets. It includes complete scene geometry, material properties, and lighting information for each scene. Also, it provides dense per-pixel semantic instance segmentations and comprehensive camera details for each image. Further, it decomposes each image into diffuse reflectance, diffuse illumination, and a non-diffuse residual component that captures view-dependent lighting effects. In terms of training split, as mentioned in the Experiments Section, we utilize the official dataset split to select approximately 54,000 samples from 365 scenes, ensuring that any incomplete samples are excluded. The RGB images and depth maps are resized to a resolution of 480×640 pixels, and the original distance measurements, defined relative to the focal point, are transformed into standard depth values relative to the focal plane.

Virtual Kitti [4, 20] Virtual KITTI is a photorealistic synthetic video dataset created for training and evaluating computer vision models on various video understanding tasks, including object detection, multi-object tracking, scene-level and instance-level semantic segmentation, optical flow, and depth estimation. The dataset comprises 50 high-resolution monocular videos (a total of 21,260 frames) generated from five distinct virtual urban environments, each presented under varying imaging and weather conditions. These virtual scenes were developed using the Unity game engine and an innovative real-to-virtual cloning technique. The synthetic videos come with precise, fully automatic annotations for 2D and 3D multi-object tracking, as well as per-pixel category, instance, flow, and depth labels.

We use its upgraded version, Virtual KITTI 2 [4], which consists of the same five sequence clones as Virtual KITTI, with increased photorealism. It takes advantage of recent advancements in lighting and post-processing within the game engine, making the variations in the virtual sequences more closely mimic real-world changes in conditions. For training, we choose four scenes, comprising around 20,000 samples, and crop the images to match the resolution of the KITTI benchmark [24]. The maximum depth is capped at 80 meters.

A.2. Evaluation Datasets

NYUv2 [69] dataset comprises 24,231 synchronized RGB images and depth maps at a resolution of 640×480 , representing various indoor scenes such as homes, offices, and commercial spaces, captured using a Microsoft Kinect. The standard split includes 249 training scenes and 215 test scenes. For our experiments, we use the official test set. Consistent with prior works [2, 35, 95–97], we exclude samples without valid ground truth, resulting in 654 valid images for evaluation. We perform evaluation on NYUv2 over a depth range spanning from 1×10^{-3} to 10 meters.

KITTI [24, 25] contains 61 driving scenes with research in autonomous driving and computer vision. It contains calibrated RGB images with synchronized point clouds from Velodyne lidar, inertial, GPS information, etc. Following prior works [2, 35, 95–97], we used Eigen split [14]. It consists of 652 testing images after filtering out images without valid ground truth. We follow the evaluation protocol of [15] for our experiments.

ScanNet [10] is an extensive RGB-D video dataset containing 2.5 million views in more than 1500 scans, annotated with 3D camera poses, surface reconstructions, and instance-level semantic segmentations. Data was collected using an RGB-D capture system (with a Kinect sensor) that includes automated surface reconstruction and crowd-sourced semantic annotation. We use the same evaluation configuration of Marigold [35], where 800 images are randomly selected from the 312 official validation scenes for evaluation.

ETH3D [68] is a multi-view stereo and 3D reconstruction benchmark encompassing a diverse range of indoor and outdoor scenes. High-precision laser scanning was used to obtain the ground truth geometry. Images were captured using both a DSLR camera and a synchronized multi-camera rig with varying fields-of-view. For evaluation, following Marigold [35], we use all 454 samples that include ground

truth depth maps.

B. Implementation Details

B.1. Visualization

When visualizing the ground truth depth map, we apply the same affine transformation we used in training. As described in the Experiments Section, we apply a linear normalization ensuring that the depth values primarily fall within the range $[-1, 1]$. The affine transformation for normalization is defined as:

$$\tilde{y}^* = \left(\frac{y^* - y_2}{y_2 - y_{98}} - 0.5 \right) \times 2, \quad (5)$$

where y_2 and y_{98} represent the 2% and 98% percentiles of the depth maps, respectively. Then, we apply min-max normalization to both the ground truth and predicted depth maps, scaling them to integer values within the range $[0, 255]$. These normalized depth maps are then visualized using the OpenCV MAGMA colormap.

It is important to note that, unlike Marigold [35], which applies linear fitting to the ground truth for error correction, we do not use this approach. While linear fitting can adjust predictions to more closely align with the ground truth, it does not accurately reflect the true distribution of the depth map predictions or provide a clear assessment of prediction quality. Instead, we enhance visualization by applying the same training normalization to the zero-shot evaluation dataset, avoiding linear fitting and its error correction effects, resulting in more authentic and insightful visualization outcomes.

B.2. Training details.

We implemented our method using PyTorch, employing Stable Diffusion v2 [63] as the backbone and maintaining the original pre-training configuration with the v -objective [65]. The training process utilized the DDPM noise scheduler [30] with 1,000 diffusion steps, while at inference time, the DDIM scheduler [71] was employed with 50 sampling steps for faster results. Our training setup spanned 30,000 iterations, with an effective batch size of 32 achieved through gradient accumulation over 16 steps (with a per-step batch size of 2) to fit on a single Nvidia RTX 3090 GPU. We used the Adam optimizer with a learning rate set at $3 \cdot 10^{-5}$ and included random horizontal flipping with a probability of 0.5 as data augmentation. For depth normalization, we employed a scale and shift-invariant method with clipping enabled and set the normalization range between -1.0 and 1.0, using a 0.02 min-max quantile to maintain robustness. This normalization strategy was applied during training and zero-shot evaluations for consistency. The training noise scheduler initialized from the pre-trained Stable Diffusion v2 [63] model maintained a noise strength

of 0.9 and incorporated an annealed strategy to progressively reduce noise levels. We saved checkpoints every 50 iterations, with backup, validation, and visualization checkpoints set at intervals of 2,000 iterations. The training process typically converged after approximately 20,000 iterations, though we extended training to 30,000 iterations for thorough coverage. We used mean squared error (MSE) as the loss function, with reduction set to “mean” for averaged loss calculation. A customized iteration-wise exponential scheduler is applied which adjusts the learning rate iteratively using an exponential decay function. It decays the learning rate to 1% of its initial value over 25,000 iterations with a warmup phase of 100 steps.

C. Additional Experiments

C.1. Visualizations

We provide additional visualization and analysis for indoor scenes in Figure 7 and outdoor scenes in Figure 8. We use several samples in the NYUv2 [69] and KITTI [24, 25] dataset across diverse types of scenes. We have provided examples in captions under each figure. These visualizations demonstrate that leveraging the language prior within the text-to-image diffusion model enhances the model’s ability to understand the geometric characteristics of the specified regions and objects. It shows that language plays a critical role in guiding the model’s attention to relevant regions and providing context for improved depth prediction. It highlights subtle or easily overlooked details, such as small objects or instances, and enhances the perception of complex scenes with multiple objects or intricate surfaces. Additionally, language descriptions offer an essential context for partially observed or occluded objects, enabling the model to infer details that visual cues alone might miss. By integrating language prior, the model achieves a more comprehensive and accurate understanding of scenes, especially in challenging scenarios.

C.2. Ablation for prompts to generate text

To mimic the language description that humans might provide to assist depth estimator during practical usage, we use the visual question-answering model LLaVA v1.6 Mistral [47]. Here we want to study the effect of different prompts. The prompt we use should elicit responses that capture essential details, including the positioning of objects, their interactions, and notable features that influence monocular depth estimation. We generate different prompts using ChatGPT 4o [52], with the prompt:

“Generate prompt for a vision-language model to generate language description for each given image in one sentence. The prompt we use needs to elicit responses that include essential details, such as the positioning of objects, their interactions, and notable features that may impact

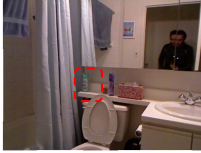


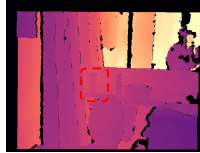
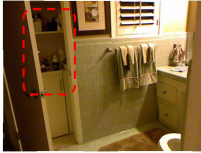


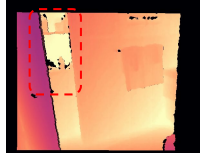

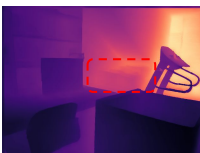

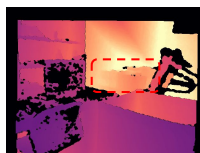
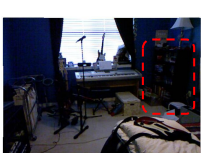

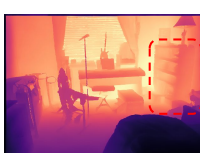

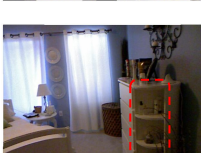

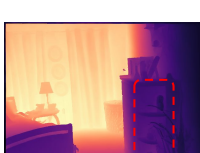

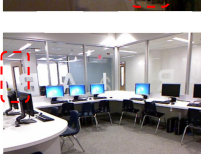
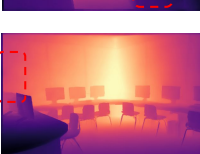
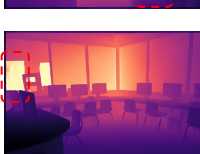
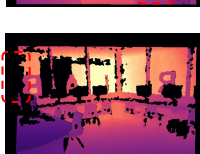
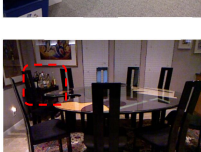
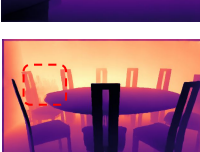

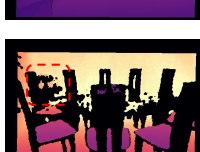
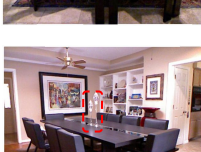
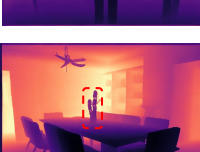
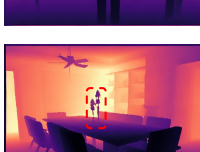
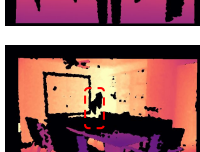
Image	Language Description	Marigold	PriorDiffusion (Ours)	Ground Truth
	The image shows a bathroom with a toilet, a green spray can , a purple bottle, sink, and mirror, with a man's reflection visible in the mirror.			
	The image shows a small, dimly lit bathroom with a toilet, sink, towel hanging on a rack, and a partially open door revealing a storage area .			
	The image shows a cluttered home office with a desk, a computer monitor, a keyboard, a chair, a cluttered space with cardboard boxes , and a child's play area with a letter 'A' on it.			
	The image shows a music-themed room with a keyboard, guitars, microphones, and other musical equipment arranged near a window with curtains, along with shelves and other furniture in the background.			
	The image shows a cozy bedroom with a white dresser , decorative plates on a blue wall, a wicker laundry basket, sheer curtains letting in soft light, and a neatly made bed with a side table.			
	The image shows a computer lab with doorway in the background and multiple desks, each equipped with a desktop computer, a monitor, and a keyboard. a			
	The image shows a formal dining room with a glass-top table surrounded by black chairs, set on a decorative rug, with artwork on the walls and a small bar cart in the corner .			
	The image shows a modern dining room with a dark wooden table, padded chairs, built-in shelves, framed artwork, two crystal ornaments on the table , and a ceiling fan.			

Figure 7. **Additional visualization on NYUv2.** Compared to Marigold, our PriorDiffusion demonstrates better depth prediction, particularly for instances specified in the language description (highlighted in red text and marked with red boxes). The language description effectively guides the model’s attention to relevant regions, especially those easily overlooked by visual cues due to a small size or a transparent texture, such as “a green spray can” in the 1st row and “two crystal ornaments” in the last row. It also improves perception under challenging visual conditions, like “shelves” in the 4th row and “a white dresser” in the 5th row, both of which are under poor illumination and are difficult to tell from visual solely. Additionally, it supports complex reasoning about scene layouts that might be misinterpreted from visual cues alone, such as “a doorway in the background” in the 6th row. Furthermore, it provides critical context for partially observed or occluded objects, such as “a partially open door revealing a storage area” in the 2nd row and “a small bar cart in the corner” in the 7th row.

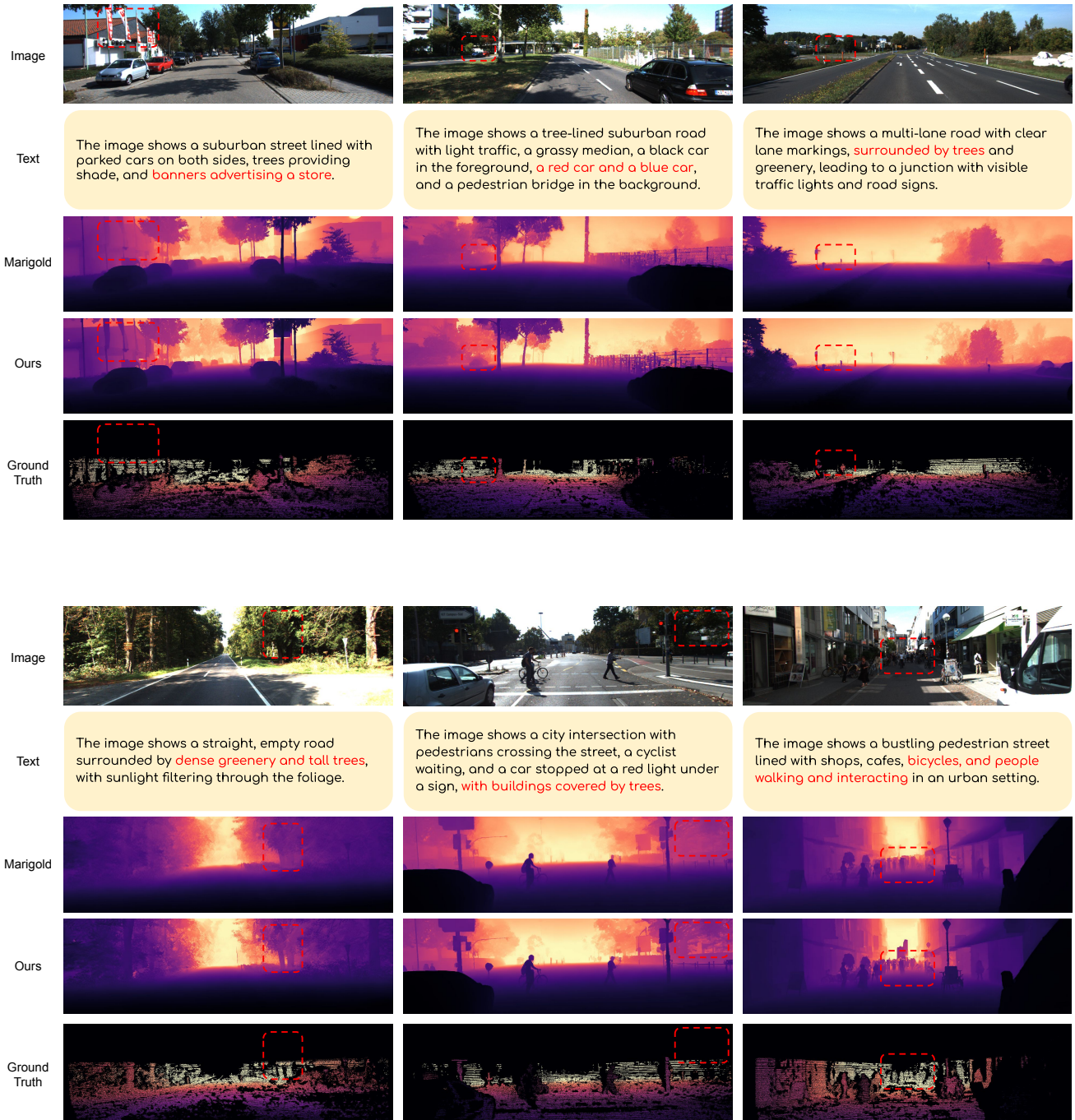


Figure 8. **Additional visualization on KITTI.** Compared to Marigold, our PriorDiffusion demonstrates superior depth prediction, particularly for instances specified in the language description (highlighted in red text and marked with red boxes). The language description effectively guides the model’s attention to relevant regions that might otherwise be overlooked due to their small size or subtle visual cues. Examples include “banners advertising a store” in the upper 1st column and “a red car and a blue car” in the upper 2nd column. Additionally, it enhances perception in complex scenes featuring multiple objects or intricate surfaces. For instance, it accurately captures “surrounded by trees” in the lower 1st column, “dense greenery and tall trees” in the upper 3rd column, and “bicycles, and people walking and interacting” in the lower 3rd column. Furthermore, the language descriptions provide essential context for partially observed or occluded objects, such as “buildings covered by trees” in the lower 2nd column.

Method	NYUv2		KITTI		ETH3D	
	$\delta_1 \uparrow$	AbsRel \downarrow	$\delta_1 \uparrow$	AbsRel \downarrow	$\delta_1 \uparrow$	AbsRel \downarrow
“An image”	95.7	6.1	89.8	10.7	95.1	6.8
Template A	95.8	6.0	90.3	10.6	95.5	6.4
Template B	95.7	6.1	90.5	10.7	95.6	6.5
Template C	95.9	6.0	90.2	10.6	95.3	6.6
Template D	95.6	5.8	90.4	10.5	95.4	6.4
Template E	95.8	5.9	90.3	10.7	95.6	6.7
Template F	95.9	6.0	90.5	10.5	95.4	6.6
Template G	95.8	6.1	90.3	10.6	95.5	6.3
Template H	95.7	5.9	90.2	10.7	95.7	6.3
Template I	95.8	6.1	90.6	10.5	95.4	6.6
Template J	95.8	6.0	90.5	10.6	95.6	6.4
Template K	95.7	5.8	90.4	10.5	95.5	6.3
Ours	95.9	5.9	90.6	10.4	95.7	6.5

Template A: “Describe the image in one sentence. Explain the image by identifying key objects and their distances from the viewpoint, noting any perspective lines or depth cues that indicate the three-dimensional structure of the scene.”

Template B: “Describe the image in one sentence. Describe the image by detailing the foreground, midground, and background objects, emphasizing their relative distances and spatial positioning within the scene.”

Template C: “Describe the image in one sentence. Describe the image by detailing the foreground, midground, and background objects, emphasizing their relative distances and spatial positioning within the scene.”

Template D: “Describe the image in one sentence. Provide an in-depth description of the image, focusing on the scale and depth of each visible object and how they overlap or are spaced from one another.”

Template E: “Describe the image in one sentence. Analyze the image by discussing the size and arrangement of objects, their positions relative to one another, and any changes in texture or clarity that indicate varying depths across the scene.”

Template F: “Describe the image in one sentence. Describe the scene with attention to depth, specifying which elements appear closer or farther from the viewer and how shadows or lighting contribute to the perception of depth.”

Template G: “Describe the image in one sentence. Highlight the depth relationships in the image by describing which objects are in the foreground, which are in the background, and how their relative sizes help convey distance.”

Template H: “Describe the image in one sentence. Focus on any natural or man-made structures in the image and describe how their orientation and placement give a sense of depth or perspective.”

Template I: “Describe the image in one sentence. Describe how elements like roads, pathways, or fences create leading lines that guide the viewer’s eye into the depth of the scene.”

Template J: “Describe the image in one sentence. Explain how differences in lighting or shadowing in the image indicate which parts are nearer or further away from the observer.”

Template K: “Describe the image in one sentence. Analyze the spatial arrangement of the main objects and describe any overlapping or occlusion that suggests depth relationships between them.”

Ours: “Describe the image in one sentence, assuming it’s a real-world image, pay more attention to objects, their spatial relationships, and the overall layout.”

Table 3. **Ablation for prompts to generate language description.** Prompts are used to prompt LLaVA to generate language descriptions for each image. While the performances among different prompts may vary, they remain consistently comparable, as long as they are meaningful and mimic human descriptions.

depth estimation.”

We present the results in Table 3, showcasing various language descriptions generated by LLaVA under different prompts. While the performances exhibit some variation, they remain consistently comparable. This demonstrates that as long as meaningful language descriptions of 3D scenes, resembling natural descriptions provided by humans, are provided, PriorDiffusion can effectively leverage the language prior to enhance monocular depth estimation.